On the Role of Aromatic Side Chains in the Photoactivation of BLUF Domains[†]

Magdalena Gauden,[‡] Jeffrey S. Grinstead,[§] Wouter Laan,[||] Ivo H. M. van Stokkum,[‡] Marcela Avila-Perez,[||] K. C. Toh,[‡] Rolf Boelens,[§] Robert Kaptein,[§] Rienk van Grondelle,[‡] Klaas J. Hellingwerf,[||] and John T. M. Kennis*,[‡]

Biophysics Group, Department of Physics and Astronomy, Faculty of Sciences, Vrije Universiteit, De Boelelaan 1081, 1081HV Amsterdam, The Netherlands, Department of NMR spectroscopy, Bijvoet Center for Biomolecular Research, Utrecht University, Padualaan 8, 3584 CH Utrecht, The Netherlands, and Swammerdam Institute for Life Science, University of Amsterdam, Nieuwe Achtergracht 166, 1018 WY Amsterdam, The Netherlands

ABSTRACT: BLUF (blue-light sensing using FAD) domain proteins are a novel group of blue-light sensing receptors found in many microorganisms. The role of the aromatic side chains Y21 and W104, which are in close vicinity to the FAD cofactor in the AppA BLUF domain from *Rhodobacter sphaeroides*, is investigated through the introduction of several amino acid substitutions at these positions. NMR spectroscopy indicated that in the W104F mutant, the local structure of the FAD binding pocket was not significantly perturbed as compared to that of the wild type. Time-resolved fluorescence and absorption spectroscopy was applied to explore the role of Y21 and W104 in AppA BLUF photochemistry. In the Y21 mutants, FADH•−W• radical pairs are transiently formed on a ps time scale and recombine to the ground state on a ns time scale. The W104F mutant shows a spectral evolution similar to that of wild type AppA but with an increased yield of signaling state formation. In the Y21F/W104F double mutant, all light-driven electron-transfer processes are abolished, and the FAD singlet excited-state evolves by intersystem crossing to the triplet state. Our results indicate that two competing light-driven electron-transfer pathways are available in BLUF domains: one productive pathway that involves electron transfer from the tyrosine, which leads to signaling state formation, and one nonproductive electron-transfer pathway from the tryptophan, which leads to deactivation and the effective lowering of the quantum yield of the signaling state formation. Our results are consistent with a photoactivation mechanism for BLUF domains where signaling state formation proceeds via light-driven electron and proton transfer from the conserved tyrosine to FAD, followed by a hydrogen-bond rearrangement and radical-pair recombination.

BLUF[1] (blue-light sensing using FAD) domains constitute a new family of flavin-based blue light photoreceptors (*1, 2*). The BLUF domain represents a novel FAD-binding fold, which alters the activity of downstream effector domains or independent effector proteins. BLUF domains are found in heterotrophic bacteria, photosynthetic bacteria, and eukaryotic algae (*2−4*). The best characterized of these proteins is AppA from the purple photosynthetic bacterium *Rhodobacter sphaeroides*. AppA functions as an antirepressor of photosynthetic gene expression, and regulates the expression of the photosynthetic machinery in response to high levels of blue light and oxygen tension (*5−7*).

Upon illumination with blue light, BLUF domains show a characteristic red shift of their absorption spectrum by approximately 10 nm, which is a unique feature of this photoreceptor family. The red-shifted species is believed to correspond to the signaling state (*6*). Transient absorption experiments on the AppA BLUF domain have revealed that the formation of the signaling state is very rapid and that it takes place in less than 1 ns (*8, 9*). The structure of the BLUF domain shows a ferredoxin-like fold consisting of a five-stranded β-sheet with two α-helices packed on one side (*10−15*). The noncovalently bound isoalloxazine ring of FAD is positioned between the two α-helices. Figure 1 shows a close up of the FAD-binding pocket. Most residues conserved among BLUF domain sequences surround the flavin chromophore, with two critical residues for the light reaction, Y21 and Q63. FTIR experiments have indicated the formation of an additional hydrogen bond at the C4 carbonyl oxygen of the FAD with a nearby amino acid in the photoactivated state (*16*). Taking these results into account, Anderson et al. proposed that photoactivation may induce an ~180° rotation of the Q63 side chain, where it may form a new additional hydrogen bond to the flavin C4═O group. In addition to the conserved tyrosine, tryptophan at position 104 is conserved among BLUF domains. Remarkably, replacement of W104 with phenylalanine (W104F) in AppA results in a 1.5-fold increased quantum yield of the signaling state formation compared to that of the wild type (*17*).

* Corresponding author. Phone: +31 20 5987937. Fax: +31 20 5987999. E-mail: john@nat.vu.nl.

[‡] Vrije Universiteit.

[§] Utrecht University.

[||] University of Amsterdam.

[1] Abbreviations: FAD, flavin adenine dinucleotide; BLUF, blue-light sensing using FAD; LOV, light, oxygen or voltage; DAS, decay associated spectrum; EADS, evolution-associated difference spectrum; SADS, species-associated difference spectrum.
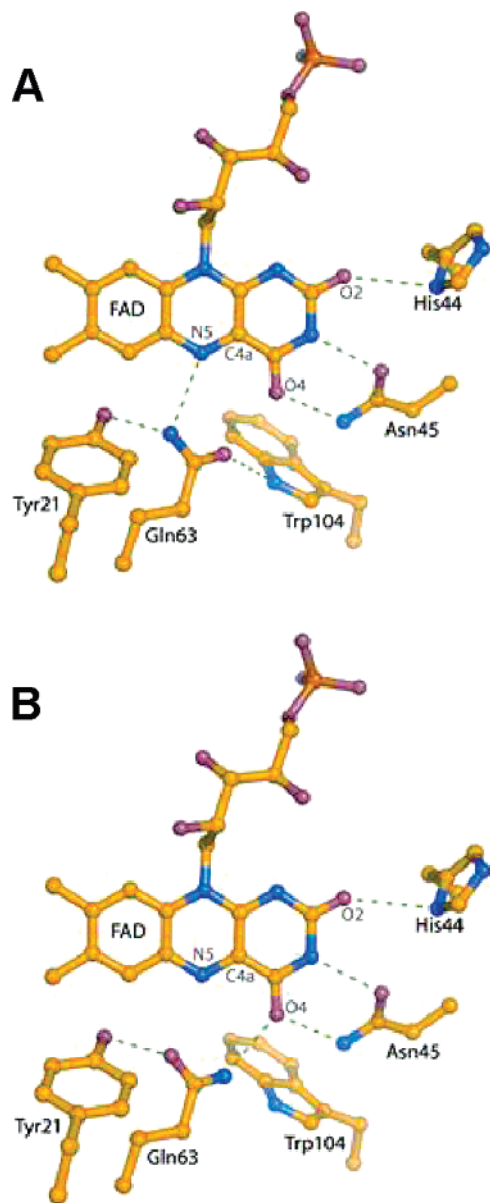
FIGURE 1: X-ray structure of the *Rb. sphaeroides* AppA BLUF domain. Panels A and B represent a close up of the vicinity of the FAD chromophore in two proposed orientations of the conserved glutamine Q63. The conserved aromatic side chains of Y21 and W104 are also indicated. The coordinates were taken from the Protein Data Bank ID code 1YRX (*10*).

In flavoenzymes, aromatic side chains in the vicinity of flavins generally are involved in electron transfer processes that drive various catalytic processes (*18*). Cryptochromes contain an array of conserved tryptophans in the vicinity of their FAD chromophore, and light-driven electron transfer from tryptophan to FAD is thought to initiate its photocycle (*19*, *20*). In contrast, no aromatic residues are located near the flavin in light, oxygen, or voltage (LOV) domains (*21*, *22*). Whether electron transfer occurs from the conserved cysteine to FMN in LOV domains is under debate as to whether it would occur slowly in microseconds, an extended time scale provided by the FMN triplet state (*23*−*32*).

It was proposed that photo-induced electron transfer from aromatic side chains to FAD would initiate the AppA photocycle (*33*, *34*). In support of this hypothesis, it was observed that the removal of tyrosine by site-directed

mutagenesis results in the inhibition of the photocycle (*35*, *36*). However, no transient FAD radicals were observed in the photocycle of dark-state AppA (*8*). Strong evidence of photo-induced electron transfer in BLUF domains was provided by ultrafast experiments on the Slr1694 BLUF domain from *Synechocystis*, where blue-light absorption was followed by the sequential formation of anionic $FAD^{\bullet-}$ and neutral FADH radicals on a picosecond time scale, demonstrating that electron transfer followed by proton transfer constitutes the BLUF photoactivation mechanism, which finally leads to the red-shifted signaling state (*37*).

Important questions regarding the role of the aromatic residues near the flavin in the mechanism of BLUF photoactivation remain. The various X-ray and NMR structures give conflicting views of the hydrogen-bond patterns that connect the FAD with the conserved glutamine, tyrosine, and tryptophan and that define the activation state of the photoreceptor. The dark state was proposed, where Q63 was oriented with its side chain amino group donating hydrogen bonds to Y21 and N5 (as in Figure 1A) (*10*, *15*) or with the amino group donating a hydrogen bond to C4=O and N5 (*11*, *12*, *14*). (AppA sequence numbering is used throughout this article.) Evidence from Raman and NMR spectroscopy favored the former (*38*, *39*). Moreover, the conformation of the tryptophan differs significantly in the various structures, with proposals for a buried conformation at 3 Å edge-to-edge distance to FAD (*10*, *13*, *15*) or a solvent-exposed conformation at considerable distance from FAD (*11*, *12*, *14*).

In this study, the role of the aromatic residues at position 21 and 104 in AppA from *Rhodobacter* (*Rb.*) *sphaeroides* is investigated through the introduction of several amino acids substitutions at these positions by site-directed mutagenesis. We have characterized the structure of the W104F mutant with NMR spectroscopy and determined the photochemistry of the W104F and several Y21 mutants utilizing ultrafast spectroscopy. The implications for the photoactivation mechanism of the BLUF domains are discussed.

MATERIAL AND METHODS

Strains and Growth Conditions. Cloning was performed using *Escherichia coli* XL1-Blue grown in LB medium according to established protocols. Protein overproduction was performed in *Escherichia coli* M15 (pREP4) grown in production broth (PB: 20 g L^{-1} tryptone, 10 g L^{-1} yeast extract, 5 g L^{-1} dextrose, 5 g L^{-1} NaCl, and 8.7 g L^{-1} K_2-HPO_4 at pH 7.0). Ampicillin and kanamycin were used at 100 and 50 μg mL^{-1}, respectively.

Site-Directed Mutagenesis. The BLUF domain with the W104F mutation was constructed with the QuickChange site-directed mutagenesis kit (Stratagene, La Jolla, CA). pQEAppA$_{5-125}$ (*36*) was used as the template for the PCR reaction using the primers AppA W104F F, 5′-GCTTTGCGGGATTT-CACATGCAGCTCTCCTGC-3′ and AppA W104F R, 5′-GCAGGAGAGCTGCATGTGAAATCCCGCAAAGC-3′.

The Y21 mutant samples were constructed with the QuickChange site-directed mutagenesis kit (Stratagene, La Jolla, CA). pQEAppA$_{5-125}$ was employed as the template for PCR, and the primer sequences were as follows:

AppA Y21I F CTGGTTTCCTGCTGCATTCGCAGC-CTGGCGGC,

AppA Y21I R GCCGCCAGGCTGCGAATGCAGCAG-GAAACCAG,

AppA Y21F F CTGGTTTCCTGCTGCTTTCGCAGC-CTGGCGGC,

AppA Y21F R GCCGCCAGGCTGCGAAAGCAGCAG-GAAACCAG,

AppA Y21C F CTGGTTTCCTGCTGCTGCCGCAGC-CTGGCGGC,

AppA Y21C R GCCGCCAGGCTGCGGCAGCAGCAG-GAAACCAG.

The double mutant was constructed by sequential mutation of Y21 and W104. All constructs were verified by sequencing (BaseClear, Leiden, The Netherlands).

Protein Production and Purification. AppA$_{5-125}$ mutants were expressed and purified essentially as described previously (*40*). Before proceeding with the nickel−resin purification, the cell-free extracts were incubated for 1 h on ice with a large molar excess of FAD. Purified proteins were dialyzed to 10 mM Tris-HCl at pH 8.0 and stored at −20 °C. Purity of the samples was checked by SDS−PAGE using PHAST-System (Amersham Biosciences) and UV−vis spectroscopy. The flavin composition of each variant was determined by thin-layer chromatography (TLC) as described earlier (*40*).

Ultrafast Time-Resolved Spectroscopy. Time-resolved fluorescence experiments were performed with the synchro-scan streak camera setup described earlier (*41*). The time-resolved fluorescence kinetics were recorded upon excitation at 400 nm at a power of 500 μW. Pulses of 100 fs duration were generated with a 50 kHz repetition rate using an amplified Ti/sapphire laser system (Vitesse-DUO-Rega, Coherent Inc., Mountain View CA). Fluorescence was collected with a right-angle detection geometry using achromatic lenses and detected through a sheet polarizer set at the magic angle (54.7°) with a Hamamatsu C5680 synchro-scan streak camera and a Chromex 250IS spectrograph. The streak images were recorded with a cooled (−55 °C) Hamamatsu C4880 CCD camera. Streak camera images were obtained on a time basis of 500 ps and 2 ns and were simultaneously analyzed. The excitation wavelength was 400 nm, and the fluorescence was monitored in a spectral window from 460 to 650 nm.

Femtosecond transient absorption spectroscopy was carried out with the 1 kHz Ti/sapphire-based regenerative amplification system described earlier (*42*). Pulsed 400 nm light, attenuated to 300 nJ, was obtained by using a frequency doubled output of the Ti/sapphire laser and was used as a pump. A white light continuum that was generated by focusing the rest of the amplified 800 nm light on a 1 mm CaF$_2$ crystal was used as a probe. Femtosecond time delays between pump and probe were controlled by a delay line covering delays up to 5 ns. During the measurements, the relative polarization of the pump and probe beams was set at the magic angle (54.7°). After passing through the sample, the probe was dispersed by a polychromator and projected on a diode array detector.

For the time-resolved absorption experiments, the Y21 mutants were loaded into a static cuvette with a pathway of 2 mm and mounted on a shaker that constantly vibrated the cuvette sideways at a frequency of 20 Hz, with an amplitude of 1 mm. The W104F mutant sample was loaded onto a flow system of 12 mL volume, including a flow cuvette of 1 mm path length, and flowed by a peristaltic pump. The absor-bance of the samples was adjusted to 0.3 per mm. The absorption spectrum of the W104F sample was checked during the measurements to verify that the sample remained in the dark state. For the time-resolved fluorescence experiments, the Y21 mutant proteins were loaded onto a flow system of 2 mL volume, where the flow cuvette had a path length of 2 mm. The absorbance of the sample was adjusted to 0.07 per mm at 446 nm.

Data Analysis. The time-resolved fluorescence data recorded on time bases of 500 ps and 2 ns were simultaneously globally analyzed in terms of a sum of exponentials to obtain decay associated spectra (DAS). The femtosecond transient absorption data were globally analyzed using a kinetic model consisting of sequentially interconverting evolution-associated difference spectra (EADS), that is, $1 \rightarrow 2 \rightarrow 3 \rightarrow ...$, in which the arrows indicate successive monoexponential decays of increasing time constants, which can be regarded as the lifetime of each EADS. The first EADS corresponds to the time-zero difference spectrum. This procedure enables us to quantify the evolution of the (excited) state(s) of the system. In general, the EADS may well reflect mixtures of molecular states. To further unravel the pathways for transient intermediate formation that follow light absorption in the AppA mutants, a target analysis was performed in which a specific kinetic scheme was tested. With this procedure, the species-associated difference spectra (SADS) of pure molecular states are estimated. The instrument response function was fit to a Gaussian of 120 fs full width half maximum for the ultrafast transient absorption experiments and 6 to 13 ps for the time-resolved fluorescence measurements when conducted on the 500 ps and 2 ns time bases, respectively. The global analysis procedures described in this article have been extensively reviewed in ref *43*.

NMR Spectroscopy. The AppA$_{5-125}$ W104F sample for NMR spectroscopy was ∼1 mM in 20 mM d$_{11}$-Tris buffer at pH 7.4. NMR spectra were recorded on a Bruker AVANCE spectrometer operating at 500 MHz. 1D NMR spectra were acquired with 100 ms acquisition time and 2048 transients, and a spectral window of 16 ppm using the WATERGATE sequence for suppression of water resonance. Spectra were recorded at 290 K. The 2D NOESY spectra were recorded as 2048 × 256 points at 290 K, with a mixing time of 50 ms. The assignment of selected proton resonances was achieved by comparison with wild type spectra (*39*). Light excitation of the protein sample within the spectrometer was achieved using an argon laser in a previously described setup (*44*) with a light intensity of 150 mW, either continuously or pulsed for 400 ms once every 1.5 s.

RESULTS

AppA W104F. NMR spectra reveal several important features of the W104F mutant of the BLUF domain of AppA. Resolved peaks in 1D ^{1}H NMR spectra appear almost identical to those of wild type AppA (Figure 2A) (*13, 39*). The high degree of similarity of these resolved peaks (including protein side chain, protein backbone amide, and FAD H3 resonances) indicates that the overall structure of AppA W104F is very similar to that of the wild type protein. Furthermore, in NOESY spectra of the AppA mutant W104F (Figure 2B), the intensity and chemical shift of NOEs to the side chain of Y21Hϵ, (I79Hγ2, V88Hγ2, I79Hδ1, V88Hγ1,
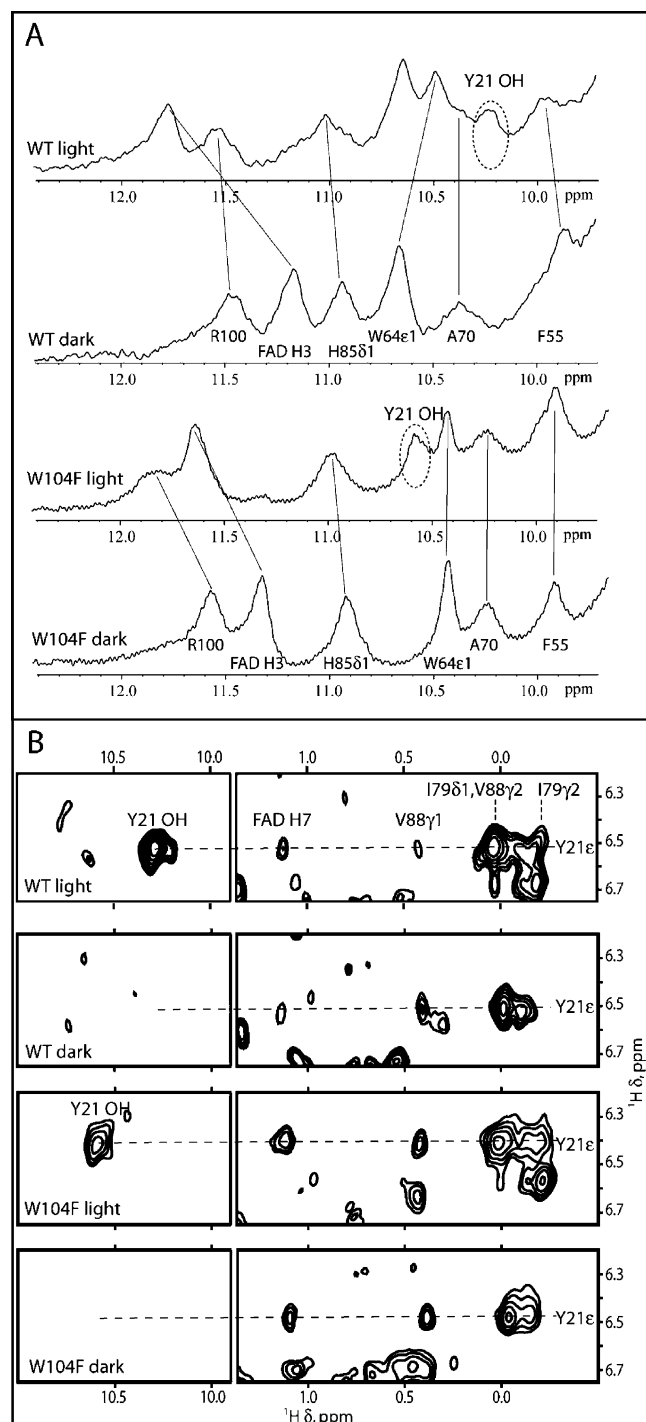
FIGURE 2: Dark and light-irradiated (A) 1D and (B) NOESY NMR spectra of AppA WT and W104F mutant proteins at 290 K. In both proteins, a resonance for Y21OH appears in response to light.

and FAD H7) are almost the same as those in the wild type spectra and indicate that the local structure around this essential side chain is not significantly perturbed by the mutation of W104.

Illumination of the W104F mutant protein results in the same changes in 1D and NOESY spectra that were observed for the wild type protein (*39*), including the appearance of a resonance for the Y21 side chain hydroxyl proton (Figure 2, light spectra). Observation of this proton resonance is consistent with the formation of a hydrogen bond to the Q63 side chain oxygen in the light-induced signaling state and
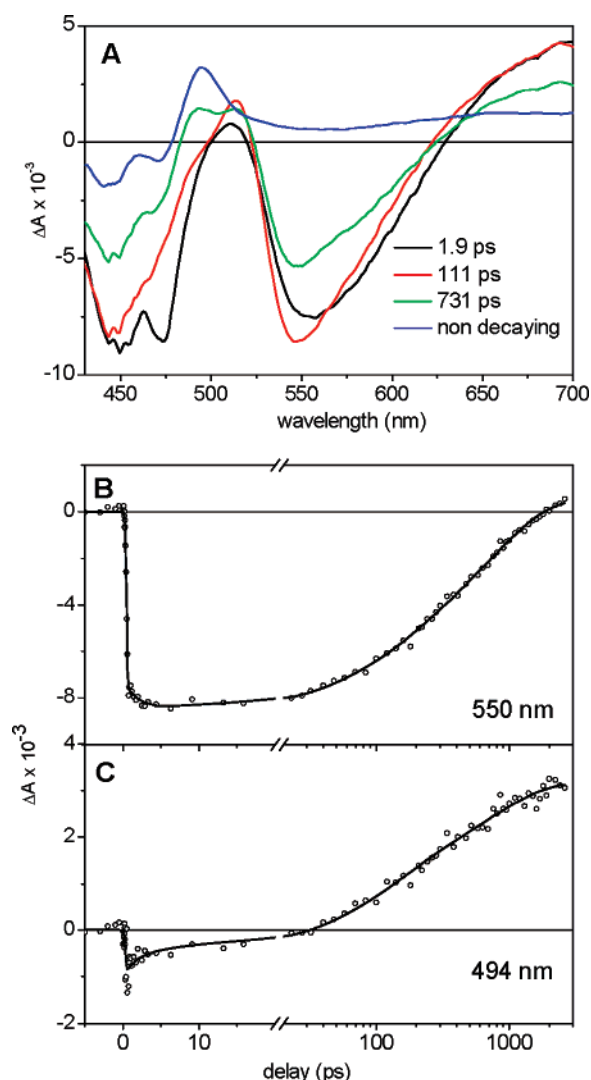

FIGURE 3: (A) Evolution-associated difference spectra (EADS) and their corresponding lifetimes resulting from the global analysis of ultrafast transient absorption experiments on the W104F AppA mutant upon 400 nm excitation. (B) Time-resolved kinetic trace detected at 550 nm (○) of the W104F AppA mutant upon 400 nm excitation, along with the result of the global analysis (—). Note that the time axis is linear from −5 to 20 ps and logarithmic thereafter. (C) Same as panel B with detection at 494 nm.

supports the model proposed by Anderson et al., where light absorption induces the flipping of Q63 (*10*).

Figure 3 shows the results from ultrafast transient absorption spectroscopy on the W104F mutant. The sample was excited at 400 nm, and the time-resolved absorbance changes were monitored over a wavelength range from 420 to 700 nm. The data were globally analyzed in terms of a kinetic scheme with sequentially interconverting species. Each species is characterized by an evolution-associated difference spectrum, EADS. Figure 3A shows the EADS, whereas kinetic traces at selected wavelengths are shown in Figure 3B and C. Four kinetic components were required in order to satisfactorily fit the data, with lifetimes of 1.9 ps, 111 ps, 731 ps, and a nondecaying component. A subpicosecond component present in the spectral evolution of wild type AppA and other BLUF domains (*8, 37*) could not be resolved as a result of a strong cross-phase modulation artifact. The first EADS with a lifetime of 1.9 ps (Figure 3A, black line) can be assigned to the hot singlet excited-state of FAD, as

in wild type AppA (*8*). This EADS evolves in 1.9 ps to the next EADS (Figure 3A, red line), which has a lifetime of 111 ps and is attributed to the relaxed FAD singlet excited state, hereafter denoted as FAD*. It exhibits spectral features similar to the previous EADS with a small increase and a blue shift of the stimulated emission band, an increase of excited-state absorption around 500 nm, and a partial loss of a vibronic feature near 475 nm. The 111 ps EADS is spectrally similar to that of FAD* in solution (*45*), wild type AppA (*8*), and FMN* in the LOV2 domain of phototropin (*9, 26*).

The next EADS, which has a lifetime of 731 ps (Figure 3A, green line), has characteristics similar to those of the previous EADS but with a decrease of ground state bleach and stimulated emission and thus corresponds to the decay of FAD*. In addition, a shoulder around 490 nm has appeared. In the fourth EADS (Figure 3A, blue line), which did not decay on the time scale of the experiment, the ground state bleach and stimulated emission have largely vanished. Instead, an absorption peak near 490 nm is formed, which resembles the absorption difference spectrum of the long-lived AppA signaling state at 495 nm. Moreover, a weak, broad absorption band is observed in the spectral region between 550 and 700 nm, which is assigned to the flavin triplet state (FAD^T). The overall spectral evolution of AppA W104F is similar to that of wild type AppA (*8*), whereas the observed excited-state lifetimes are slightly longer (111 and 730 ps vs 90 and 590 ps for W104F and wild type, respectively), as evident from time-resolved fluorescence experiments (*17*).

Comparison of the amplitude of the product formed in the last nondecaying EADS near 495 nm versus the amplitude of the ground state bleach of FAD* shortly after excitation (111 ps EADS) can be used as a relative measure of the quantum yield of the signaling state formation. In the W104F mutant, this ratio is 1.6 times larger than that in wild type AppA. The quantum yield of the signaling state formation in wild type AppA was previously shown to amount to 24% (*8*). Thus, the estimated quantum yield of the signaling state formation in W104F amounts to 38%, which is in good agreement with the 37% value determined by actinometric methods (*17*). Figure S1 in Supporting Information shows the results of a target analysis on the W104F mutant utilizing a kinetic model identical to that applied to wild type AppA (*8*).

AppA Y21 Mutants. Synchroscan streak camera experiments were performed to examine the FAD excited-state decay of the Y21 AppA mutants. A global analysis procedure applied to Y21I mutant data yielded four decay components of 7.5 ps, 45 ps, 354 ps, and 3.5 ns. Figure 4A shows the decay associated spectra (DAS) that resulted from the application of global analysis. Similar to wild type AppA and the *Synechocystis* Slr1694 BLUF domain, FAD* decays in a multiexponential fashion (*8, 37*). The 45 ps component is dominant with a decay amplitude of 0.41, with smaller contributions made by the 7.5 ps (amplitude 0.30) and 354 ps (amplitude 0.22) components. The longest component of 3.5 ns has the smallest contribution (amplitude 0.07) and probably follows from a minor fraction of free FAD, judged from the fluorescence maximum peaking around 530 nm. The DAS of the Y21C and Y21F mutants were similar and are shown in Figure S2 in Supporting Information, and the
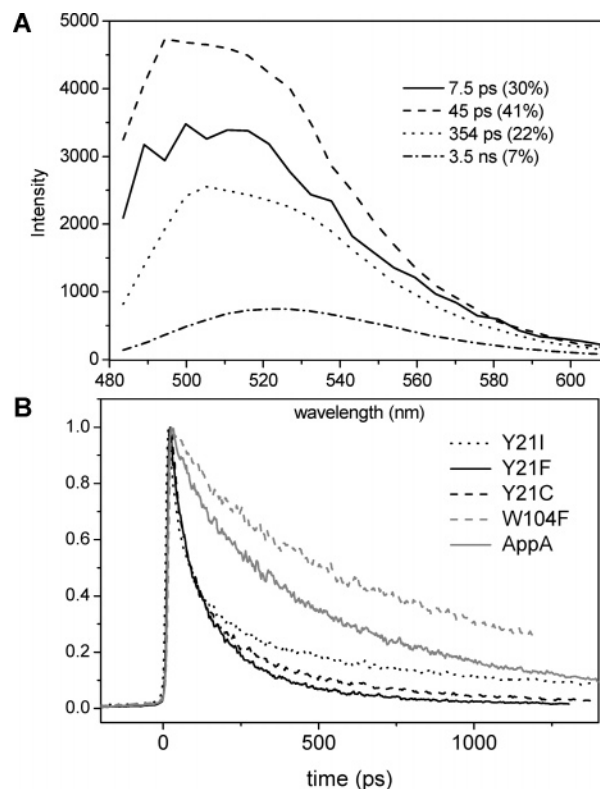

FIGURE 4: (A) Decay associated spectra (DAS) and associated time constants that follow from a global analysis of the streak camera image obtained from the Y21I AppA mutant upon 400 nm excitation. (B) Time-resolved fluorescence trace recorded at 505 nm of the Y21I (black dotted line), Y21F (black line), Y21C (black dashed line) and W104F mutants (gray dashed line), and wild type AppA (gray line).

lifetimes and amplitudes are shown in Table 1. Kinetic traces detected at 505 nm near the maximum of the fluorescence emission of the Y21I, Y21F, Y21C, and W104F mutants and wild type AppA are depicted in Figure 4B. It is striking that the FAD* lifetime in all three Y21 mutants is much shorter than that in wild type AppA, where lifetimes of 25 ps, 150 ps, 670 ps, and 3.8 ns were observed. The dominant component in the wild type is 670 ps, whereas in the Y21 mutants, the second component (<55 ps) dominates the fluorescence decay.

To examine the photochemistry of the Y21 mutants in more detail, femtosecond time-resolved absorption spectroscopy was performed. The excitation wavelength was 400 nm. The EADS that result from the sequential analysis on Y21I are presented in Figure 5A, whereas kinetic traces (circles) at selected wavelengths are shown in Figure 5B−F along with the result of the global fit (solid lines). Six components were required for an adequate description of the time-resolved data, with lifetimes of 460 fs, 3 ps, 14 ps, 56 ps, 300 ps, and 5.8 ns. The 460 fs (Figure 5A, black curve) and 3 ps (Figure 5A, red curve) EADS were observed in wild type AppA as well and were ascribed to a mixture of initially created FAD S_1 and S_2 singlet excited states and to the hot FAD S_1 excited state, respectively (*8*). The latter EADS evolves in 3 ps to the next EADS (Figure 5A, green curve), which has a lifetime of 14 ps. It can be assigned to the relaxed S_1 singlet excited-state of the FAD chromophore, FAD*. This EADS evolves in 14 ps to the next EADS (Figure 5A, blue line), which has a lifetime of 56 ps. The

Table 1: Rate Constants and Fractional Contributions that Result from an Analysis of the Ultrafast Fluorescence Time-Resolved Data on AppA Mutants

Y21C	Y21I	Y21F
$k_1 = (7 \text{ ps})^{-1}$ $F_1 = 0.22$	$k_1 = (7.5 \text{ ps})^{-1}$ $F_1 = 0.41$	$k_1 = (7.5 \text{ ps})^{-1}$ $F_1 = 0.17$
$k_2 = (50 \text{ ps})^{-1}$ $F_2 = 0.46$	$k_2 = (45 \text{ ps})^{-1}$ $F_2 = 0.3$	$k_2 = (55 \text{ ps})^{-1}$ $F_2 = 0.42$
$k_3 = (268 \text{ ps})^{-1}$ $F_3 = 0.3$	$k_3 = (354 \text{ ps})^{-1}$ $F_3 = 0.22$	$k_3 = (212 \text{ ps})^{-1}$ $F_3 = 0.4$
$k_4 = (4.2 \text{ ns})^{-1}$ $F_4 = 0.02$	$k_4 = (3.5 \text{ ns})^{-1}$ $F_4 = 0.07$	$k_4 = (7.1 \text{ ns})^{-1}$ $F_4 = 0.01$

latter EADS shows a decrease of the stimulated emission band and an increase of absorption around 510 and 610 nm. The ground state bleach has slightly decreased compared to that of the previous EADS. Thus, the 56 ps EADS corresponds to a remaining fraction of FAD* and a significant contribution from another molecular species. In fact, this EADS is similar to that observed on the same time scale in the *Synechocystis* Slr1694 BLUF domain, where neutral flavin semiquinone radicals were shown to be transiently present (*37*). The temporal behavior of the radical species is shown in the kinetic trace at 606 nm (Figure 5E), where FAD* has an isosbestic point. The trace starts near zero, and on the time scale of picoseconds, the radical species gives rise to a positive signal, after which it decays to near zero on a (sub) ns time scale.

The evolution in 56 ps to the next EADS (Figure 5A, cyan line), which has a lifetime of 300 ps, corresponds to an almost complete loss of the stimulated emission band and partial loss of the ground state bleach. The induced absorption bands at 510 and 600 nm have remained. In the fifth EADS (Figure 5A, magenta line), which has a lifetime of 5.6 ns, the ground state bleach has largely disappeared, and an additional species with a broad absorption ranging from 500 to 700 nm is formed. On the basis of previous studies on flavins, the broad, positive signal of the long-lived component at wavelengths longer than 500 nm can be assigned to FAD^T (*25*, *26*). The final EADS of the Y21I mutant has low amplitude, which indicates that the majority of the neutral flavin semiquinone radicals return to the original ground state of oxidized FAD. Note that the lifetime of the final EADS, 5.6 ns, is uncertain as it decays on a time scale similar to the maximum time position of the setup's optical delay line (4.8 ns).

It was shown before that mutation of Y21 inhibited the formation of the signaling state (*35*, *36*). Consistently, the absorption band around 495 nm that corresponds to the signaling state formation is not observed in the present data on Y21I. The EADS and lifetimes that resulted from the sequential analysis of Y21F and Y21C are similar to those obtained with Y21I (results not shown). The lifetimes and spectral evolution roughly agree with those observed earlier by Dragnea et al. with the Y21F mutant (*33*), although no rigorous global analysis was performed in the latter work.

Target Analysis on AppA Y21I: Identification of Transient FADH•−W• Radical Pairs. The femtosecond transient absorption data on AppA Y21 mutants confirm that there is no direct formation of the long-lived signaling state from the electronically excited state but instead a transient formation of other product(s). At all times during the photoreaction, the time-resolved spectra consist of a mixture of multiple molecular species, that is, FAD* and, presumably, FAD radicals. To disentangle these contributions, we performed a target analysis of the time-resolved data. A detailed description of this method is provided in ref *43*. Applying the target analysis will allow identification of the spectral

characteristics of all species in the form of a species-associated difference spectrum (SADS), estimation of their lifetimes, and their connectivity. The kinetic model that we used in the target analysis to disentangle the contribution of the FAD* and other species is shown in Figure S3 in Supporting Information. It consists of seven compartments: FAD$_{HOT}$, three FAD* species, a transient product Q, a transient product R, and the FAD triplet state FAD^T.

The decay of FAD* is highly multiexponential in AppA mutants (see the streak camera data of Figure 4, and also note that stimulated emission from FAD* is present in the first four EADS in the sequential model in Figure 5). This is most likely caused by the presence of conformational substates in the dark, as revealed for wild type AppA by NMR spectroscopy (*13*). The heterogeneity in the FAD* decay is accounted for in the target analysis by assuming three compartments with different decay times but identical spectra, denoted as FAD*$_{1-3}$. The SADS of FAD^T was implemented from our previous experiment on wild type AppA (*8*).

The initially created hot S$_1$ of FAD cools in ~1 ps (rate constant k_1). Relaxation from FAD$_1^*$ and FAD$_2^*$ occurs primarily through Q. FAD$_2^*$ also has a relaxation channel (45%) to the ground state (rate constant k_9), whereas FAD$_3^*$ entirely decays to the ground state (rate constant k_4). From FAD*$_{1,2,3}$, a small fraction undergoes intersystem crossing to FAD^T at a fixed rate of $k_T = (5 \text{ ns})^{-1}$. Q decays to R by rate constant k_6 but is also allowed to generate FAD^T by k_5 and to decay to the ground state by k_7. R entirely decays to the ground state. The rate constants and FAD-decay fractions, estimated from the target analysis on the Y21 mutants, are summarized in Table S1 in Supporting Information.

Figure 6A shows the species-associated difference spectra (SADS) of FAD*, Q, R, and FAD^T resulting from the kinetic modeling on the data obtained with the Y21I mutant. As expected, the SADS of FAD* (Figure 6A, red line) has the typical spectral shape of the singlet-excited state as determined previously for AppA (*8*) and as follows from the sequential analysis in Figure 5A. Decay of FAD*$_1$, FAD*$_2$, and FAD*$_3$ takes place with time constants of 15, 69, and 315 ps, respectively. These values are in good agreement with the values obtained from the time-resolved fluorescence experiment shown in Figure 4A. The fractional contributions from FAD*$_1$, FAD*$_2$, and FAD*$_3$ in the two experiments are nearly identical, with contributions of 34%, 34%, and 32% respectively, derived from the target analysis.

Upon decay of FAD*, the Q species is formed, which lives for 290 ps. The SADS of Q (Figure 6A, blue line) has a broad absorption in the 480−650 nm region with peaks at 510 and 600 nm. This SADS resembles the absorption difference spectrum of a neutral semiquinone flavin radical observed in a number of flavoenzymes, FADH• (*46*), and it is observed in the photoreaction of the *Synechocystis* Slr1694 BLUF domain (*37*). We note that for an FADH• species,
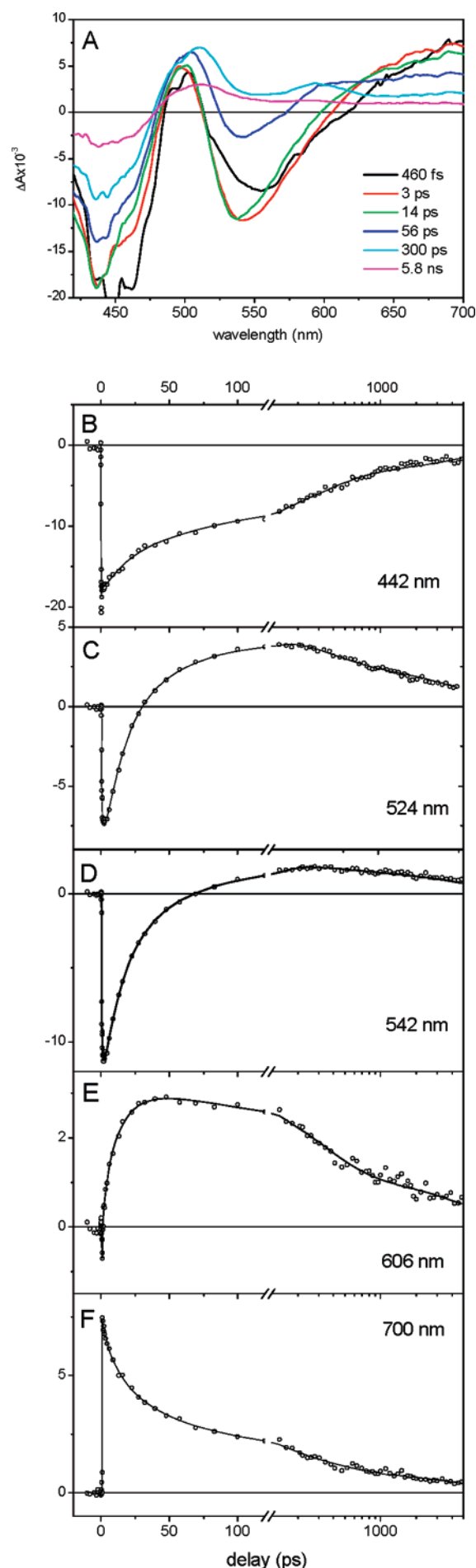
the absorption amplitude of Q at 510 nm is relatively high as compared to that at 600 nm, which suggests a contribution of another molecular species absorbing in the 500 nm region. Tryptophanyl neutral radicals (W•) are known to have an absorption in this spectral region with an extinction coefficient of 3700 M^{-1} cm^{-1} (47, 48). Thus, the spectral signature of the Q species is consistent with that of a radical pair FADH•−W•.

The R species is less straightforward to assign. Its SADS (Figure 6A, green line) features a ground-state bleach near 450 nm and an induced absorption near 500−520 nm, and it is essentially zero at wavelengths longer than 550 nm. It has a lifetime of 2 ns, after which it decays to the ground state. The ground state bleach near 450 nm indicates that R corresponds to a flavin species. Its spectral shape, with a low absorption to the red side of the oxidized flavin roughly corresponds to that of an anionic flavin semiquinone radical FAD•− (49) to which it is tentatively assigned. The induced absorption near 520 nm has roughly the same amplitude as the ground state bleach near 450 nm and is significantly higher than that expected for anionic semiquinones. It is at a wavelength similar to that observed for the neutral semiquinone Q, which suggests that here too the tryptophanyl neutral radical W• may have a contribution. If this were the case, the proton coming off FADH• would have an acceptor different from W104.

Thus, application of target analysis on the Y21I mutant resulted in a separation of FAD*, a neutral semiquinone−tryptophanyl radical pair FADH•−W•, a putative semiquinone anionic radical FAD•−, and an FAD triplet state. Figure 6B represents a reaction scheme that Y21 mutants follow after blue-light excitation. We conclude that electron and proton transfer from W104 to FAD constitute the primary light-triggered events, leading to the formation of the radical pair FADH•−W• with multiple time constants of 15 and 69 ps. From the present data, we cannot deduce whether electron, proton, or hydrogen transfer is the rate-limiting reaction. However, in wild type AppA and the *Synechocystis* Slr1694 BLUF domain, the excited-state lifetime was found to be insensitive to deuteration (17, 37), indicating that electron transfer to FAD constitutes the rate-limiting event; we presume that this is the case here as well. The radical pair largely recombines to the ground state via proton back-shuttling from the flavin to W104 or another acceptor in 290 ps, resulting in the anionic FAD•− radical, which finally decays to the ground state in 2 ns. From FAD* and FADH•, the flavin triplet state FAD^T is formed at low yield at an intersystem crossing rate of (5 ns)$^{-1}$ and (3.7 ns)$^{-1}$, respectively. These dynamics are reminiscent of those observed in glucose oxidase, where light-driven electron/proton transfer and subsequent radical pair recombination among FAD and aromatic side chains was found to occur on time scales similar to those reported here (50). In contrast to glucose

FIGURE 5: (A) Evolution-associated difference spectra (EADS) and their corresponding lifetimes resulting from the global analysis of ultrafast transient absorption experiments on the Y21I AppA mutant upon 400 nm excitation. (B) Time-resolved kinetic trace detected at 442 nm (○) upon 400 nm excitation, along with the result of the global analysis (−). Note that the time axis is linear from −15 to 120 ps and logarithmic thereafter. (C−F) Same as panel B, with detection at 524, 542, 606, and 700 nm, respectively.
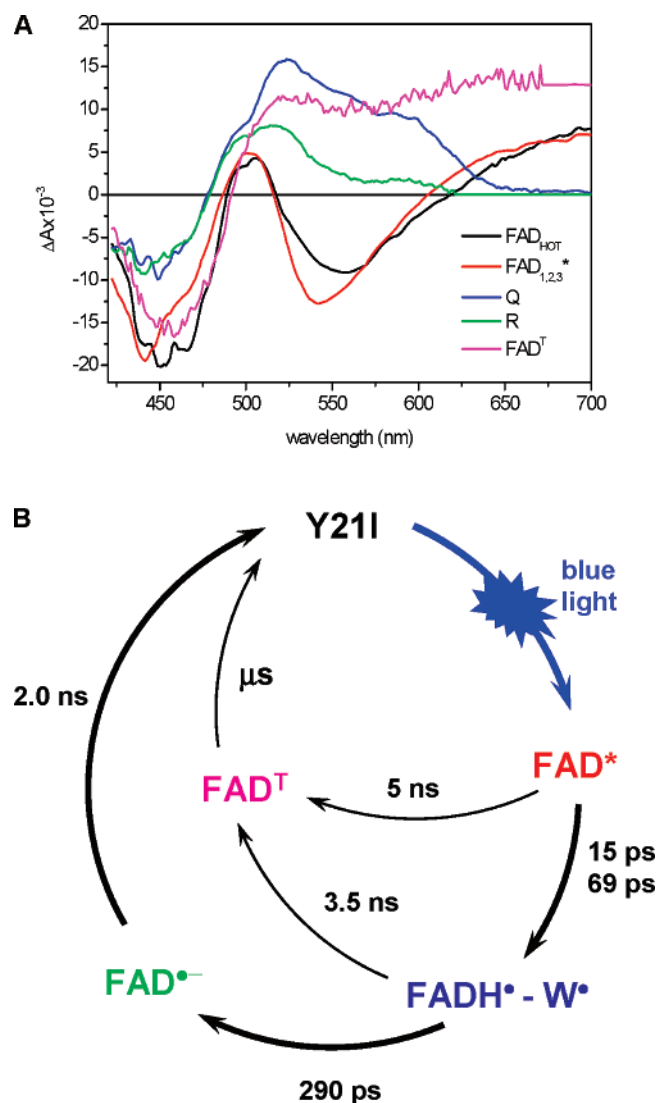
FIGURE 6: (A) Species-associated difference spectra (SADS) of various molecular species that were estimated from the application of a target analysis to the transient absorption data on the Y21I AppA mutant. (B) Simplified kinetic reaction scheme for the data obtained with the Y21I AppA mutant. See text for details.
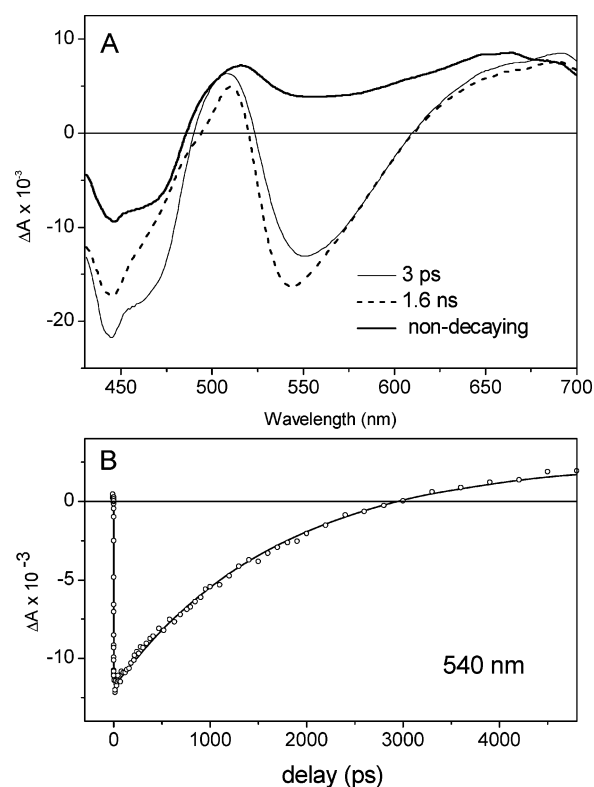

FIGURE 7: (A) Evolution-associated difference spectra (EADS) and their corresponding lifetimes resulting from the global analysis of ultrafast transient absorption experiments on the Y21F/W104F AppA mutant upon 400 nm excitation. (B) Time-resolved kinetic trace detected at 540 nm (○) of the Y21F/W104F AppA mutant upon 400 nm excitation, along with the result of the global analysis (—).

oxidase, no stable, long-lived FADH• species could be generated in the Y21 mutants by anaerobic photoreduction (data not shown).

Y21F/W104 Double Mutant. Next, femtosecond transient absorption experiments were performed on the double mutant in which both aromatic residues in the vicinity of FAD were replaced by phenylalanine (i.e., the Y21F/W104F mutant). The EADS that result from the sequential analysis of the resulting data are shown in Figure 7A. Three kinetic components were required to fit the data, with lifetimes of 3 ps (thin solid line) and 1.6 ns (dashed line), and a nondecaying component (thick solid line). As with the W104F mutant (Figure 3), a subpicosecond component present in the spectral evolution could not be resolved as a result of a strong cross-phase modulation artifact.The first two EADS, with lifetimes of 3 ps and 1.6 ns, represent the unrelaxed and relaxed FAD singlet excited states, respectively. Strikingly, the FAD singlet excited-state lifetime of 1.6 ns in the double mutant is significantly longer than that in wild type AppA and 2 orders of magnitude longer than that in Y21 mutants. The nondecaying EADS can be assigned

to the FAD triplet state (*8*, *25*), which implies that upon excitation, FAD* only undergoes ISC to the triplet state and internal conversion to the ground state. In fact, the overall spectral evolution of the double mutant is very similar to that observed in the LOV2 domain of phototropin (*26*). Thus, all light-driven electron-transfer processes in AppA are abolished upon replacement of Y21 and W104 by an amino acid with a less favorable midpoint potential for electron transfer to the flavin. The absence of additional intermediates demonstrates that Y21 and W104 are entirely and solely responsible for the initiation of the productive and nonproductive photochemistry of BLUF domains.

Figure 7B shows a kinetic trace recorded at 540 nm, the wavelength with maximal sensitivity to stimulated emission from FAD*. Importantly, FAD* in the wild type and W104F and Y21 mutants decays multiexponentially, whereas in the double mutant, FAD* decays monoexponentially with a time constant of 1.6 ns. This observation further supports our previous interpretation of the origin of the multiexponential decay of FAD* in wild type AppA (*8*) and the Y21 and W104 single mutants (this work, vide supra). The slow time scale (μs−ms) exchange of the conserved Y and W residues between different conformational states (*13*) very likely leads to subpopulations having variations in the distance between FAD and the aromatic residues, with an ensuing distribution of (fast) electron-transfer rates as a result.

DISCUSSION

We have characterized the photochemistry of AppA mutants in which the aromatic residues Y21 and W104 have
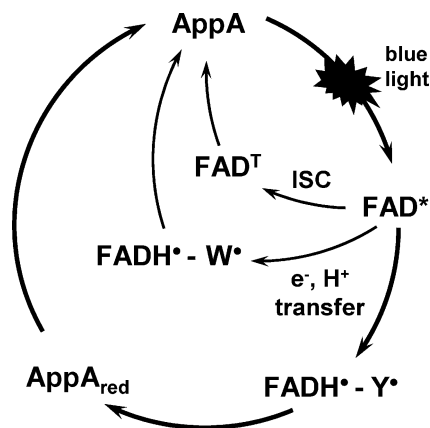
FIGURE 8: Photoactivation scheme of the AppA BLUF domains, with a productive reaction pathway through electron/proton transfer from Y21 to FAD that results in the signaling state AppA$_{red}$ and a nonproductive pathway via electron/proton transfer from W104 to FAD that leads to radical pair recombination to the original ground state on an ultrafast time scale. The intersystem crossing pathway to the FAD triplet state is also included.

been replaced by amino acids with a less-favorable midpoint potential for electron transfer to the flavin with ultrafast spectroscopy. We have demonstrated, utilizing NMR spectroscopy, that the structure of the W104F mutant is very similar to that of the wild type BLUF domain, in particular in the vicinity of the FAD chromophore. Despite the inability of Y21 mutants to generate the signaling state, a transient neutral semiquinone−tryptophanyl FADH$^\bullet$−W$^\bullet$ radical pair appears, which recombines to the ground state on a nanosecond time scale, likely via a FAD$^{\bullet-}$ radical species. Previous studies on flavo enzymes revealed that light-driven electron transfer from aromatic residues to the flavin often constitutes their photochemistry(*50, 51*). The redox properties of the flavin and the surrounding aromatic side chains define the driving force for electron transfer. Because phenylalanine and isoleucine cannot undergo redox chemistry under physiological conditions, W104, which is located at 3 Å from FAD (edge to edge) (*10, 13*), most likely acts as the electron and proton donor in the Y21 mutants. This assignment was confirmed by the results on the Y21F/W104F double mutant, where blue-light excitation only results in direct evolution from FAD* to FAD^T on a nanosecond time scale via intersystem crossing. Furthermore, replacement of these two aromatic residues results in complete suppression of the BLUF photochemistry. The W104F (single) mutant undergoes a photocycle and signaling state formation similar to that of wild type AppA, demonstrating that W104 is not required for AppA photoactivation. In the W104F mutant, the lifetime of the singlet excited state of FAD is prolonged, and the quantum yield of the signaling state formation is larger than that in the wild type, as reported earlier (*14*).

The results from ultrafast spectroscopy for the Y21 and W104 mutants and wild type AppA can be rationalized in terms of the photoactivation scheme depicted in Figure 8. Upon excitation of wild type AppA, two competing pathways for electron transfer to FAD* are available to the system: (i) a productive pathway that involves electron and proton transfer from Y21 to FAD and that results in the formation of the long-lived signaling state, a view consistent with earlier work on the Slr1694 BLUF domain from *Synechocystis* (*37*),

and (ii) a nonproductive pathway, which involves electron and proton transfer from W104 to FAD, resulting in the transient formation of a FADH$^\bullet$−W$^\bullet$ radical pair. This radical pair recombines to the ground state on a ps−ns time scale and thus forms a deactivation pathway that is decoupled from signaling-state formation. Upon removal of Y21, the long-lived signaling state is not formed, but photo-induced electron and proton transfer to the flavin still occurs from W104. In contrast, upon removal of W104, the signaling state is still being generated by photo-induced electron and proton transfer from Y21. The quantum yield for this process is increased because in this mutant the competing deactivation pathway provided by electron transfer from W104 has been eliminated. Upon removal of both Y21 and W104, all light-driven electron and proton-transfer processes are abolished, and FAD* only decays by intersystem crossing to the triplet state and internal conversion to the ground state.

The observed electron/proton-transfer processes from W104 to FAD in the Y21 mutants and the competing electron-transfer deactivation pathway from W104 to FAD in wild type indicate that W104 must be located in close vicinity to FAD. Our results are consistent with a buried conformation of W104 as identified by X-ray crystallography and NMR spectroscopy by Anderson et al. and by Grinstead et al. (*10, 13, 39*). Tryptophan fluorescence experiments on the Slr1694 BLUF domain indeed indicate such a buried conformation (*15*). Other X-ray structures of BLUF domains have indicated a solvent-exposed tryptophan at a great distance from FAD (*11, 12, 14*). No appreciable electron transfer on picosecond timescales is expected to occur in such cases.

The notion that light-induced electron transfer to the flavin can occur from either Y21 or W104 is consistent with results from NMR spectroscopy of the wild type (*13*), Y21F (*35*), and W104F proteins (this work). The similarity of their NMR spectra allows us to conclude that the overall structure of the W104F mutant is comparable to that of wild type AppA. Specifically, the distance from Y21 to the flavin in the W104F protein is about the same as that in the NMR and X-ray structures of the wild type protein (*10, 13*). Therefore, the absence of W104 does not affect the structure of the residues involved in electron transfer. Our observation in the W104F mutant that Q63 flips (i.e., rotates its side chain amide group by 180°) upon illumination to form a hydrogen bond between its side chain oxygen and Y21OH is identical to the behavior in the wild type protein (*39*) and provides strong evidence that even though W104 in the wild type AppA is available to hydrogen bond to Q63 in the dark, this hydrogen bond is not necessary for the formation of the light-induced signaling state. This hydrogen bond also appears unimportant for stabilizing the dark state conformation of the Q63 side chain. Thus, our results are consistent with a photo-activation mechanism for BLUF domains where signaling state formation proceeds via light-driven electron and proton transfer from the conserved tyrosine to FAD, followed by a glutamine flip, hydrogen-bond rearrangement, and radical-pair recombination (*37*).

Although the occurrence of light-driven electron-transfer processes in wild type AppA and in several mutants are roughly additive, depending on the presence of Y21 and W104, the rates at which they proceed are clearly not. In the Y21 mutants, the FAD* lifetime is an order of magnitude

shorter than that in wild type AppA, which indicates that the rate of electron transfer from W104 to FAD* is much faster than that in the wild type. However, the rate of radical-pair recombination appears to be faster in wild type as compared to that in the Y21 mutants because no transient radicals are observed in the photoreaction of the former (*8*). These phenomena may stem from an alteration of the redox potential of FAD or decreased donor−acceptor distances upon removal of Y21. An altered donor−acceptor distance upon removal of Y21 is supported by NMR spectra of Y21F (*35*), which is missing upfield-shifted aliphatic resonances. These resonances were assigned in the WT protein to I79 and I37 side chain aliphatic protons (*13*), which pack tightly against the isoalloxazine ring of the flavin. Disappearance or shifting of these resonances indicates that the packing of the flavin in the core of the protein has been disturbed, which could also lead to a reduction in the distance between the flavin ring and the W104 side chain, thereby allowing faster electron transfer in the Y21 mutants. It is probable that the Y21F protein has lost a hydrogen bond from the Q63 side chain to flavin N5. This would have the effect of a blue-shift of the UV−vis absorbance spectrum, which is observed in absorbance spectra of the Y21F mutant (*35*, *36*). Loss of the N5 hydrogen bond also would alter the redox potential of the flavin and therefore would alter the kinetics of electron transfer from nearby W104. Additionally, the loss of rigid packing between the flavin ring and the helices could allow a reduction in the average distance between the flavin and W104 side chain, thereby allowing faster electron transfer in the Y21 mutants.

The observation that the quantum yields of signaling state formation in wild type AppA and the W104F mutant are not 100% implies that deactivation processes other than those described above must be active in the AppA BLUF domain. In the *Synechocystis* Slr1694 BLUF domain, it was observed that charge recombination following initial electron transfer from the conserved tyrosine (i.e., electron back-transfer from FAD$^{\bullet-}$) leads to a loss of ∼50−60% of the productive radical pairs FADH$^{\bullet}$−Y$^{\bullet}$ (*37*). We suppose that a similar phenomenon occurs in AppA.

CONCLUSIONS

In this work, we have shown that both Y21 and W104 act as electron and proton donors to FAD in the AppA BLUF domain and its mutants. In wild type AppA, a competition between electron transfer from Y21 and W104 to FAD underlies productive and nonproductive reaction pathways, respectively. Removal of W104 does not noticeably alter the local structure around the FAD chromophore, but eliminates the nonproductive electron-transfer pathway, and the quantum yield of signaling state formation is increased accordingly. The removal of Y21 results in impairment of the photocycle, but transient formation of a FADH$^{\bullet}$−W$^{\bullet}$ radical pair occurs on the ps time scale, which recombines to the ground state on the ns time scale. Removal of both Y21 and W104 abolishes all light-induced electron-transfer processes, demonstrating that these two aromatic residues are responsible for the initiation of all of the photochemistry of the BLUF domain. Finally, our results are consistent with a buried conformation of W104 in close vicinity to FAD in (dark state) wild type AppA and in the Y21 mutants.

SUPPORTING INFORMATION AVAILABLE

Kinetic model and resulting SADS of a target analysis on time-resolved absorption data from the W104F mutant; DAS from streak camera experiments on the Y21F and Y21C mutants; kinetic model applied for target analysis of time-resolved absorption data from the Y21I mutant; and a Table with resulting rate constants and branching fractions. This material is available free of charge via the Internet at http://pubs.acs.org.

REFERENCES

1. van der Horst, M. A., and Hellingwerf, K. J. (2004) Photoreceptor proteins, "star actors of modern times": a review of the functional dynamics in the structure of representative members of six different photoreceptor families, *Acc. Chem. Res. 37*, 13−20.
2. Gomelsky, M., and Klug, G. (2002) BLUF: a novel FAD-binding domain involved in sensory transduction in microorganisms, *Trends Biochem. Sci. 27*, 497−500.
3. Iseki, M., Matsunaga, S., Murakami, A., Ohno, K., Shiga, K., Yoshida, K., Sugai, M., Takahashi, T., Hori, T., and Watanabe, M. (2002) A blue-light-activated adenylyl cyclase mediates photoavoidance in *Euglena gracilis*, *Nature 415*, 1047−1051.
4. Rajagopal, S., Key, J. M., Purcell, E. B., Boerema, D. J., and Moffat, K. (2004) Purification and initial characterization of a putative blue light-regulated phosphodiesterase from *Escherichia coli*, *Photochem. Photobiol. 80*, 542−547.
5. Braatsch, S., Gomelsky, M., Kuphal, S., and Klug, G. (2002) A single flavoprotein, AppA, integrates both redox and light signals in *Rhodobacter sphaeroides*, *Mol. Microbiol. 45*, 827−836.
6. Masuda, S., and Bauer, C. E. (2002) AppA is a blue light photoreceptor that antirepresses photosynthesis gene expression in *Rhodobacter sphaeroides*, *Cell 110*, 613−623.
7. Gomelsky, M., and Kaplan, S. (1998) AppA, a redox regulator of photosystem formation in *Rhodobacter sphaeroides* 2.4.1, is a flavoprotein: identification of a novel FAD binding domain, *J. Biol. Chem. 273*, 35319−35325.
8. Gauden, M., Yeremenko, S., Laan, W., van Stokkum, I. H. M., Ihalainen, J. A., van Grondelle, R., Hellingwerf, K. J., and Kennis, J. T. M. (2005) Photocycle of the flavin-binding photoreceptor AppA, a bacterial transcriptional antirepressor of photosynthesis genes, *Biochemistry 44*, 3653−3662.
9. Kennis, J. T. M., and Alexandre, M. T. A. (2006) in *Flavins* (Edwards, A. M., Ed.) pp 287−319, RSC Publishing, Cambridge, U.K.
10. Anderson, S., Dragnea, V., Masuda, S., Ybe, J., Moffat, K., and Bauer, C. (2005) Structure of a novel photoreceptor, the BLUF domain of AppA from *Rhodobacter sphaeroides*, *Biochemistry 44*, 7998−8005.
11. Kita, A., Okajima, K., Morimoto, Y., Ikeuchi, M., and Miki, K. (2005) Structure of a cyanobacterial BLUF protein, Tll0078, containing a novel FAD-binding blue light sensor domain, *J. Mol. Biol. 349*, 1−9.
12. Jung, A., Domratcheva, T., Tarutina, M., Wu, Q., Ko, W. H., Shoeman, R. L., Gomelsky, M., Gardner, K. H., and Schlichting, L. (2005) Structure of a bacterial BLUF photoreceptor: insights into blue light-mediated signal transduction, *Proc. Natl. Acad. Sci. U.S.A. 102*, 12350−12355.
13. Grinstead, J. S., Hsu, S. T. D., Laan, W., Bonvin, A., Hellingwerf, K. J., Boelens, R., and Kaptein, R. (2006) The solution structure of the AppA BLUF domain: insight into the mechanism of light-induced signaling, *ChemBioChem 7*, 187−193.
14. Jung, A., Reinstein, J., Domratcheva, T., Shoeman, R. L., and Schlichting, I. (2006) Crystal structures of the AppA BLUF domain photoreceptor provide insights into blue light-mediated signal transduction, *J. Mol. Biol. 362,* 717−732.
15. Yuan, H., Anderson, S., Masuda, S., Dragnea, V., Moffat, K., and Bauer, C. (2006) Crystal structures of the *Synechocystis* photoreceptor Slr1694 reveal distinct structural states related to signaling, *Biochemistry 45*, 12687−12694.
16. Masuda, S., Hasegawa, K., Ishii, A., and Ono, T. (2004) Light-induced structural changes in a putative blue-light receptor with a novel FAD binding fold sensor of blue-light using FAD (BLUF); Slr1694 of *Synechocystis* sp PCC6803, *Biochemistry 43*, 5304−5313.

17. Laan, W., Gauden, M., Yeremenko, S., van Grondelle, R., Kennis, J. T. M., and Hellingwerf, K. J. (2006) On the mechanism of activation of the BLUF domain of AppA, *Biochemistry 45*, 51–60.

18. Ghisla, S., and Massey, V. (1989) Mechanisms of flavoprotein-catalyzed reactions, *Eur. J. Biochem. 181*, 1–17.

19. Giovani, B., Byrdin, M., Ahmad, M., and Brettel, K. (2003) Light-induced electron transfer in a cryptochrome blue-light photoreceptor, *Nat. Struct. Biol. 10*, 489–490.

20. Zeugner, A., Byrdin, M., Bouly, J. P., Bakrim, N., Giovani, B., Brettel, K., and Ahmad, M. (2005) Light-induced electron transfer in *Arabidopsis* cryptochrome-1 correlates with in vivo function, *J. Biol. Chem. 280*, 19437–19440.

21. Crosson, S., and Moffat, K. (2001) Structure of a flavin-binding plant photoreceptor domain: Insights into light-mediated signal transduction, *Proc. Natl. Acad. Sci. U.S.A. 98*, 2995–3000.

22. Fedorov, R., Schlichting, I., Hartmann, E., Domratcheva, T., Fuhrmann, M., and Hegemann, P. (2003) Crystal structures and molecular mechanism of a light-induced signaling switch: The Phot-LOV1 domain from *Chlamydomonas reinhardtii*, *Biophys. J. 84*, 2474–2482.

23. Kay, C. W. M., Schleicher, E., Kuppig, A., Hofner, H., Rudiger, W., Schleicher, M., Fischer, M., Bacher, A., Weber, S., and Richter, G. (2003) Blue light perception in plants: detection and characterization of a light-induced neutral flavin radical in a C450A mutant of phototropin, *J. Biol. Chem. 278*, 10973–10982.

24. Schleicher, E., Kowalczyk, R. M., Kay, C. W. M., Hegemann, P., Bacher, A., Fischer, M., Bittl, R., Richter, G., and Weber, S. (2004) On the reaction mechanism of adduct formation in LOV domains of the plant blue-light receptor phototropin, *J. Am. Chem. Soc. 126*, 11067–11076.

25. Swartz, T. E., Corchnoy, S. B., Christie, J. M., Lewis, J. W., Szundi, I., Briggs, W. R., and Bogomolni, R. A. (2001) The photocycle of a flavin-binding domain of the blue light photoreceptor phototropin, *J. Biol. Chem. 276*, 36493–36500.

26. Kennis, J. T. M., Crosson, S., Gauden, M., van Stokkum, I. H. M., Moffat, K., and van Grondelle, R. (2003) Primary reactions of the LOV2 domain of phototropin, a plant blue-light photoreceptor, *Biochemistry 42*, 3385–3392.

27. Sato, Y., Iwata, T., Tokutomi, S., and Kandori, H. (2005) Reactive cysteine is protonated in the triplet excited state of the LOV2 domain in Adiantum phytochrome3, *J. Am. Chem. Soc. 127*, 1088–1089.

28. Kottke, T., Heberle, J., Hehn, D., Dick, B., and Hegemann, P. (2003) Phot-LOV1: photocycle of a blue-light receptor domain from the green alga *Chlamydomonas reinhardtii*, *Biophys. J. 84*, 1192–1201.

29. Dittrich, M., Freddolino, P. L., and Schulten, K. (2005) When light falls in LOV: a quantum mechanical/molecular mechanical study of photoexcitation in Phot-LOV1 of *Chlamydomonas reinhardtii*, *J. Phys. Chem. B. 109*, 13006–13013.

30. Kottke, T., Dick, B., Fedorov, R., Schlichting, I., Deutzmann, R., and Hegemann, P. (2003) Irreversible photoreduction of flavin in a mutated Phot-LOV1 domain, *Biochemistry 42*, 9854–9862.

31. Losi, A., Polverini, E., Quest, B., and Gartner, W. (2002) First evidence for phototropin-related blue-light receptors in prokaryotes, *Biophys. J. 82*, 2627–2634.

32. Domratcheva, T., Fedorov, R., and Schlichting, I. (2006) Analysis of the primary photocycle reactions occurring in the light, oxygen, and voltage blue-light receptor by multiconfigurational quantum-chemical methods, *J. Chem. Theory Comput. 2*, 1565–1574.

33. Dragnea, V., Waegele, M., Balascuta, S., Bauer, C., and Dragnea, B. (2005) Time-resolved spectroscopic studies of the AppA blue-light receptor BLUF domain from *Rhodobacter sphaeroides*, *Biochemistry 44*, 15978–15985.

34. Zirak, A., Penzkofer, A., Schiereis, T., Hegemann, P. A. J., and Schlichting, I. (2005) Absorption and fluorescence spectroscopic characterization of BLUF domain of AppA from *Rhodobacter sphaeroides*, *Chem. Phys. 315*, 142–154.

35. Kraft, B. J., Masuda, S., Kikuchi, J., Dragnea, V., Tollin, G., Zaleski, J. M., and Bauer, C. E. (2003) Spectroscopic and mutational analysis of the blue-light photoreceptor AppA: A novel photocycle involving flavin stacking with an aromatic amino acid, *Biochemistry 42*, 6726–6734.

36. Laan, W., van der Horst, M. A., van Stokkum, I. H., and Hellingwerf, K. J. (2003) Initial characterization of the primary photochemistry of AppA, a blue-light-using flavin adenine dinucleotide-domain containing transcriptional antirepressor protein from *Rhodobacter sphaeroides*: a key role for reversible intramolecular proton transfer from the flavin adenine dinucleotide chromophore to a conserved tyrosine? *Photochem. Photobiol. 78*, 290–297.

37. Gauden, M., van Stokkum, I. H. M., Key, J. M., Luhrs, D. C., Van Grondelle, R., Hegemann, P., and Kennis, J. T. M. (2006) Hydrogen-bond switching through a radical pair mechanism in a flavin-binding photoreceptor, *Proc. Natl. Acad. Sci. U.S.A. 103*, 10895–10900.

38. Unno, M., Masuda, S., Ono, T., and Yamauchi, S. (2006) Orientation of a key glutamine residue in the BLUF domain from AppA revealed by mutagenesis, spectroscopy, and quantum chemical calculations, *J. Am. Chem. Soc. 128*, 5638–5639.

39. Grinstead, J. S., Avila-Perez, M., Hellingwerf, K. J., Boelens, R., and Kaptein, R. (2006) Light-induced flipping of a conserved glutamine sidechain and its orientation in the AppA BLUF domain, *J. Am. Chem. Soc. 128*, 15066–15067.

40. Laan, W., Bednarz, T., Heberle, J., and Hellingwerf, K. J. (2004) Chromophore composition of a heterologously expressed BLUF-domain, *Photochem. Photobiol. Sci. 3*, 1011–1016.

41. Gobets, B., van Stokkum, I. H. M., Rogner, M., Kruip, J., Schlodder, E., Karapetyan, N. V., Dekker, J. P., and van Grondelle, R. (2001) Time-resolved fluorescence emission measurements of photosystem I particles of various cyanobacteria: a unified compartmental model, *Biophys. J. 81*, 407–424.

42. Gradinaru, C. C., Kennis, J. T. M., Papagiannakis, E., van Stokkum, I. H. M., Cogdell, R. J., Fleming, G. R., Niederman, R. A., and van Grondelle, R. (2001) An unusual pathway of excitation energy deactivation in carotenoids: singlet-to-triplet conversion on an ultrafast timescale in a photosynthetic antenna, *Proc. Natl. Acad. Sci. U.S.A. 98*, 2364–2369.

43. van Stokkum, I. H. M., Larsen, D. S., and van Grondelle, R. (2004) Global and target analysis of time-resolved spectra, *Biochim. Biophys. Acta 1657*, 82–104.

44. Bernard, C., Houben, K., Derix, N. M., Marks, D., van der Horst, M. A., Hellingwerf, K. J., Boelens, R., Kaptein, R., and van Nuland, N. A. J. (2005) The solution structure of a transient photoreceptor intermediate: delta 25 photoactive yellow protein, *Structure 13*, 953–962.

45. Stanley, R. J. (2001) Advances in flavin and flavoprotein optical spectroscopy, *Antioxid. Redox Signaling 3*, 847–866.

46. Müller, F., Brüstlein, M., Hemmerich, P., Massey, V., and Walker, W. H. (1972) Light-absorption studies on neutral flavin radicals, *Eur. J. Biochem. 25*, 573–580.

47. Solar, S., Getoff, N., Surdhar, P. S., Armstrong, D. A., and Singh, A. (1991) Oxidation of tryptophan and *N*-methylindole by N3$^\bullet$, Br2$^{\bullet-}$, and (Scn)2$^{\bullet-}$ radicals in light-water and heavy-water solutions: a pulse-radiolysis study, *J. Phys. Chem. 95*, 3639–3643.

48. Aubert, C., Vos, M. H., Mathis, P., Eker, A. P. M., and Brettel, K. (2000) Intraprotein radical transfer during photoactivation of DNA photolyase, *Nature 405*, 586–590.

49. Miura, R. (2001) Versatility and specificity in flavoenzymes: control mechanisms of flavin reactivity, *Chem. Rec. 1*, 183–194.

50. Zhong, D. P., and Zewail, A. H. (2001) Femtosecond dynamics of flavoproteins: charge separation and recombination in riboflavine (vitamin B-2)-binding protein and in glucose oxidase enzyme, *Proc. Natl. Acad. Sci. U.S.A. 98*, 11867–11872.

51. Mataga, N., Chosrowjan, H., Shibata, Y., Tanaka, F., Nishina, Y., and Shiga, K. (2000) Dynamics and mechanisms of ultrafast fluorescence quenching reactions of flavin chromophores in protein nanospace, *J. Phys. Chem. B 104*, 10667–10677.